Article

Cite This: *Biomacromolecules* 2018, 19, 3586−3593

pubs.acs.org/Biomac

Construction of Small-Sized, Robust, and Reduction-Responsive Polypeptide Micelles for High Loading and Targeted Delivery of Chemotherapeutics

Song Xue, Xiaolei Gu, Jian Zhang, Huanli Sun, Chao Deng,* and Zhiyuan Zhong*

Biomedical Polymers Laboratory, and Jiangsu Key Laboratory of Advanced Functional Polymer Design and Application, College of Chemistry, Chemical Engineering and Materials Science, Soochow University, Suzhou 215123, People's Republic of China

Supporting Information

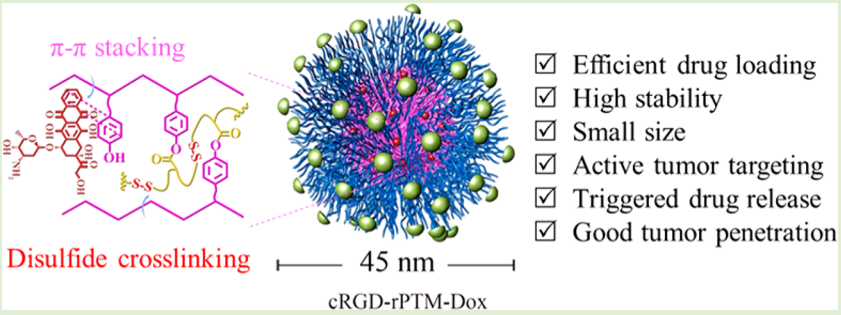

ABSTRACT: Polypeptide micelles, though having been proved to be an appealing nanoplatform for cancer chemotherapy, are met with issues like inefficient drug encapsulation, gradual drug release, and low tumor cell selectivity and uptake. Here, we report on cRGD-decorated, small-sized, robust, and reduction-responsive polytyrosine micelles (cRGD-rPTM) based on poly(ethylene glycol)-*b*-poly(L-tyrosine)-lipoic acid (PEG-*b*-PTyr-LA) conjugate for high loading and targeted delivery of doxorubicin (Dox). Notably, cRGD-rPTM exhibited efficient loading of Dox, giving cRGD-rPTM-Dox with a drug loading content (DLC) of 18.5 wt % and a small size of 45 nm at a theoretical DLC of 20 wt %. cRGD-rPTM-Dox displayed reduction-triggered drug release, high selectivity and superior antiproliferative activity toward $\alpha_v\beta_3$ integrin positive MDA-MB-231 breast cancer cells (IC_{50} = 1.5 μg/mL) to both nontargeted rPTM-Dox and clinical liposomal formulation (LP-Dox). cRGD-rPTM-Dox demonstrated a prolonged circulation time compared with the noncrosslinked cRGD-PTM-Dox control and significantly better accumulation in MDA-MB-231 breast tumor xenografts than nontargeted rPTM-Dox. Moreover, cRGD-rPTM-Dox at 6 mg Dox equiv/kg could remarkably suppress growth of MDA-MB-231 human breast tumor without inducing obvious side effects, outperforming both rPTM-Dox and LP-Dox. These reduction-responsive multifunctional polytyrosine micelles appear to be a viable and versatile nanoplatform for targeted chemotherapy.

INTRODUCTION

Polymeric micelles with a lipophilic core are an ideal nanocarrier system for lipophilic anticancer drugs.[1−3] Among all micelles, polypeptide micelles have attracted particular interest because polypeptides are known to possess good biocompatibility, biodegradability, and tunable structures and functions.[4−9] Notably, several polypeptide micellar drugs, for example, with paclitaxel (PTX, NK105), doxorubicin (Dox, NK911), or cisplatin (NC-6004), are under clinical investigation for treating cancerous patients.[10] The results signify that polypeptide micelles could significantly reduce drug side effects, though leading to only moderate improvement in treatment efficacy.[11,12] The therapeutic efficacy is mainly compromised by drug leakage during circulation, low tumor cell selectivity and uptake, and gradual drug release at tumor sites.[13−15]

Drug leakage from polymeric micelles can be substantially inhibited by the crosslinking of micelles.[14,16,17] In particular, disulfide-crosslinking is appealing, as it can not only increase stability, but also achieve fast drug release in cancer cells.[18−21] Several groups demonstrated that disulfide-crosslinked polypeptide-based micelles could be developed by the introduction of disulfide bond-containing crosslinkers (cystamine, 3,3′-dithiolbis(sulfosuccinimidyl propionate)) in polypeptide blocks[22,23] or oxidizing free thiol groups in poly(L-cysteine), poly(*β*-mercaptoethylamine-L-aspartic acid), poly(*γ*-(4-((2-mercaptoethyl)aminomethyl)benzyl)-L-glutamate), and dithiobispropionimidate-functionalized poly(L-lysine) blocks.[24−27] Disulfide-crosslinked nanoparticles have also been developed through direct ring-opening (co)polymerization of cystine N-carboxyanhydride (cystine-NCA).[28−30] These disulfide-crosslinked polypeptide-based nanomedicines, though having shown enhanced treatment of different tumor models, including MDA-MB-231 breast cancer, A549 lung cancer,

Received: May 25, 2018
Revised: July 18, 2018
Published: July 19, 2018

DOI: 10.1021/acs.biomac.8b00835
Biomacromolecules 2018, 19, 3586−3593

Scheme 1. cRGD-Decorated, Small-Sized, Robust, and Reduction-Responsive Polypeptide Micelles (cRGD-rPTM) Developed from Poly(ethylene glycol)-*b*-poly(L-tyrosine)−Lipoic Acid Conjugate (PEG-*b*-PTyr-LA) for Efficient Encapsulation and Targeted Delivery of Doxorubicin

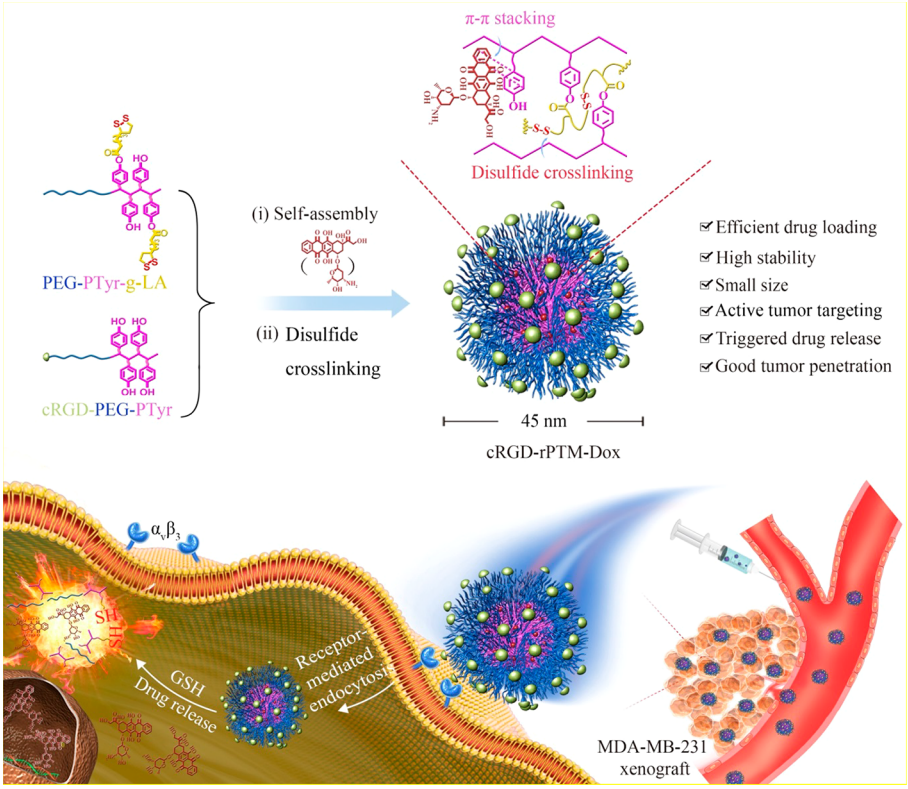

HepG hepatoma, and human T24 bladder cancer, are often perplexed by ill-controlled polymerization, tedious postpolymerization modification, and moderate drug loading.

Here, we report facile preparation of small-sized, robust and reduction-responsive polytyrosine micelles from poly(ethylene glycol)-*b*-poly(L-tyrosine)-lipoic acid (PEG-*b*-PTyr-LA) conjugates for tumor-targeted delivery of Dox (Scheme 1). Recently, we have demonstrated that polypeptide micelles developed from PEG-*b*-PTyr displayed a high loading of Dox through $\pi-\pi$ stacking though drug-encapsulated micelles had rather big sizes varying from 97 to 181 nm, depending on Dox contents.[31] LA is a natural antioxidant and has been utilized to enable reversible disulfide-crosslinking of polymeric micelles in previous studies.[32−34] Interestingly, our present studies show that PEG-*b*-PTyr-LA with a short PTyr of 2.0 kg/mol and conjugation of four units of LA per chain afforded disulfide-crosslinked micelles with a small size (45 nm), superb drug loading, and reduction-responsive drug release. We used cRGD peptide, which can selectively bind to $\alpha_v\beta_3$ and $\alpha_v\beta_5$ receptors on cancer cells,[35−38] as a model targeting ligand, to explore the in vitro and in vivo performance of the smart polytyrosine micelles.

EXPERIMENTAL SECTION

Synthesis of PEG-*b*-PTyr-LA Diblock Polymers. PEG-*b*-PTyr diblock copolymer with an M_n of 5.0−2.0 kg/mol was simply synthesized via polymerization of L-tyrosine-*N*-carboxyanhydride (Tyr-NCA), as previously reported,[31] except that a lower molar ratio of Tyr-NCA monomer to PEG-NH_2 initiator of 13.5/1 was employed. LA was conjugated to PEG-*b*-PTyr by esterification reaction with lipoic acid anhydride (LAA) with the help of dimethylaminopyridine (DMAP). To a solution of LAA (105 mg, 266 μmol) in anhydrous DMF were added PEG-*b*-PTyr (320 mg, 45.7 μmol) and DMAP (6.5 mg, 53.3 μmol) under N_2. The reaction proceeded at 30 °C for 24 h under stirring. The product was obtained by precipitation in cold diethyl ether and purified by redissolving in chloroform and precipitating in excess diethyl ether twice. Yield: 80.7%. ^{1}H NMR (400 MH_Z, DMSO-d_6, Figure 1A, δ): 9.07 (1H, -C_6H_4-O**H**), 7.95 (1H, -**H**NCH(CH_2)CO-), 7.17, 6.96, 6.59 (4H, -C_6H_4-), 4.42 (1H, -HNC**H**(CH_2)CO-), 3.51 (4H, -CH_2CH_2O-; -S-S-C**H**-), 3.16 (2H, -HNCH(CH_2)CO-; 2H, -S-S-CH_2-), 2.41−1.44 (10H, LA moieties).

cRGD-PEG-*b*-PTyr was prepared by NCA polymerization using allyl-PEG-NH_2 as an initiator as above, followed by thiol−ene click reaction with cRGD-SH under UV irradiation. Typically, to a solution of allyl-PEG-*b*-PTyr (200 mg, 28.6 μmol) in DMF were added cRGD-SH (33.9 mg, 57.1 μmol) and Irgacure 2959 photoinitiator (4.0 mg, 17.8 μmol) under nitrogen atmosphere, followed by UV irradiation for 15 min in ice−water bath. The product was purified via extensive dialysis against DMF (MWCO 3500), and then precipitation in cold diethyl ether. Yield: 70.5%. ^{1}H NMR (400 MH_Z, DMSO-d_6, Figure 1B, δ): 9.07 (1H, -C_6H_4-O**H**), 7.95 (1H, -**H**NCH(CH_2)CO-), 7.10−7.22 (cRGD moieties), 6.91, 6.54 (4H, -C_6H_4-OH), 4.38 (1H, -HNC**H**(CH_2)CO-), 3.50 (4H, -CH_2-CH_2-O-), 2.75 (2H, -HNCH-(CH_2)CO-).

Micelle Formation and Drug Loading. Micelles were formed by dropping a solution of PEG-*b*-PTyr-LA in DMF (100 μL) to 900 μL of HEPES buffer (10 mM, pH 7.4) under stirring, followed by dialyzing against HEPES buffer (MWCO 3500). To accomplish disulfide crosslinking, a solution of dithiothreitol (DTT, 20 mol.% of lipoyl units) was added into the above micelle dispersions. The micelle dispersion was mounted in a shaking bed (100 rpm) at 37 °C for 24 h. The crosslinked micelles (rPTM) were obtained by dialyzing against HEPES buffer for 24 h. Similarly, cRGD-rPTM was prepared from PEG-*b*-PTyr-LA and cRGD-PEG-*b*-PTyr at a molar ratio of 4:1. The stability of micelles was assessed against extensive dilution or 10% fetal bovine serum (FBS). Reduction-sensitivity of micelles was

DOI: 10.1021/acs.biomac.8b00835
Biomacromolecules 2018, 19, 3586−3593

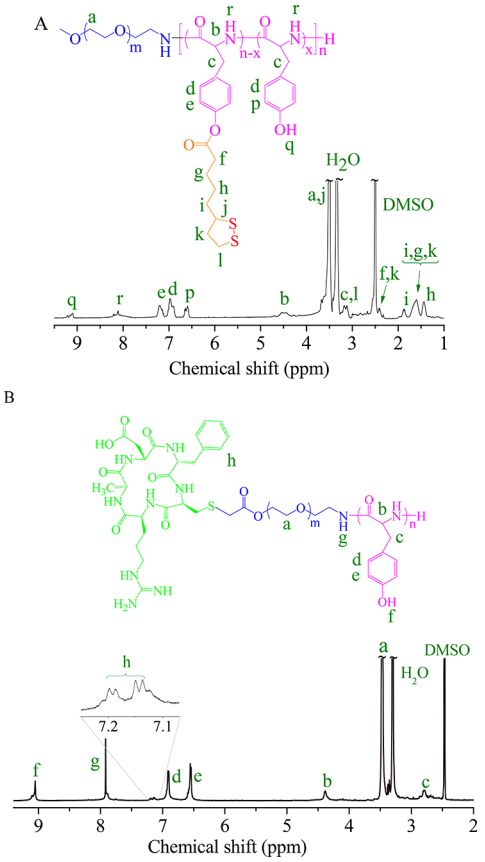

Figure 1. ^{1}H NMR spectra (400 MHz, DMSO-d_6) of (A) PEG-*b*-PTyr-LA and (B) cRGD-PEG-*b*-PTyr.

monitored by measuring their size changes against 10 mM GSH solution using DLS.

Dox encapsulation into micelles was accomplished by dropping a solution of Dox, PEG-*b*-PTyr-LA, and cRGD-PEG-*b*-PTyr (theoretical drug loading contents 5−20%) in DMF to HEPES buffer under stirring, followed by dialyzing against HEPES buffer to remove unloaded Dox. To acquire the drug loading capacity, we dissolved Dox-loaded micelles (cRGD-rPTM-Dox) in a GSH solution (10 mM) in DMF. The amount of Dox was measured using fluorescence spectrometry (FLS 920, UK), and the drug loading content (DLC) as well as drug loading efficiency (DLE) were assessed as previously reported.[39,40]

In Vivo Antitumor Efficacy. The mice were handled under protocols approved by Soochow University Laboratory Animal Center and the Animal Care and Use Committee of Soochow University. In vivo antitumor efficacy was carried out in MDA-MB-231 tumor-bearing mice. Upon the tumor size increased to around 100 mm^3, the mice were divided into four groups and intravenously injected with PBS, cRGD-rPTM-Dox, rPTM-Dox, and Lipo-Dox, respectively. Mice in each group were administrated every 4 days for a total of four injections. cRGD-rPTM-Dox and rPTM-Dox were given at a dosage of 6 mg Dox equiv/kg, while the dosage of Lipo-Dox decreased to 4 mg Dox equiv/kg considering its high systemic toxicity. Tumor sizes were determined using the formula: $V = 0.5 \times L \times W \times W$, where L and W are the length and width of tumors, respectively. The relative tumor volumes were normalized by the initial ones. At day 24, the tumor blocks were collected and weighed. Tumor inhibition rate (TIR) in each group was determined based on the formula: TIR (%) = (1 − (mean tumor weight of treated group/mean tumor weight of PBS group)) × 100.

RESULTS AND DISCUSSION

Synthesis of PEG-*b*-PTyr-LA and cRGD-PEG-*b*-PTyr Copolymer. PEG-*b*-PTyr-LA was prepared by esterification of tyrosine units in PEG-*b*-PTyr with LAA in the presence of DMAP. PEG-*b*-PTyr was obtained with an M_n of 5.0−2.0 kg/mol, according to a previously reported procedure.[31] ^{1}H NMR of PEG-*b*-PTyr-LA detected signals attributable to LA (δ 1.44−2.41), in addition to PEG-*b*-PTyr (δ 6.59, 6.96, 7.17, and 3.51; Figure 1A). Notably, signals at δ 7.17 were assigned to ortho-protons of phenyl groups in PTyr following conjugation of LA. The number of LA moieties per polymer chain could be determined by comparing the integrals of δ 7.17 with 6.59 (*ortho*-protons of tyrosine units without LA conjugation) or δ 7.17 (*meta*-protons of tyrosine units). Interestingly, PEG-*b*-PTyr-LA conjugates with 4.3 and 8.2 units of LA per chain were obtained at LAA/PEG-*b*-PTyr molar feed ratios of 6/1 and 12/1, respectively (Table 1). GPC measurements revealed that both PEG-*b*-PTyr-LA conjugates had a narrow molecular weight distribution ($Đ$ < 1.2). Hereafter, PEG-*b*-PTyr-LA$_4$ was employed for micelle preparation.

cRGD-PEG-*b*-PTyr was prepared by NCA polymerization using α-allyl-ω-amine-PEG as an initiator, followed by thiol−ene click reaction with cRGD-SH under UV radiation similar to previous reports.[36,41] ^{1}H NMR spectrum of cRGD-PEG-*b*-PTyr clearly displayed besides the peaks of PEG and PTyr pronounced signals at δ 7.10−7.22 attributable to the aromatic protons of cRGD moieties, indicating successful conjugation of cRGD (Figure 1B). The determination of cRGD, through 9,10-phenanthraquinone method,[40] showed a functionality of 91%.

Micelle Preparation and Drug Loading. Previously, we have demonstrated that polypeptide micelles developed from PEG-*b*-PTyr with an M_n of 5.0−4.9 kg/mol displayed a high loading of Dox through $\pi-\pi$ stacking, in which the sizes of micelles ranged from 97 to 181 nm depending on drug loading contents.[31] Here, PEG-*b*-PTyr-LA copolymer with a much shorter hydrophobic PTyr block (2.0 kg/mol) was employed to prepare small-sized, robust, reduction-responsive, and tumor-targeted micelles. Through adding PEG-*b*-PTyr-LA and cRGD-PEG-*b*-PTyr copolymers (molar ratio = 4:1) in HEPES buffer, the polymers co-self-assembled into cRGD-PTM, which was further self-crosslinked with the help of DTT to form cRGD-rPTM. UV−vis measurement displayed that the absorption of dithiolane ring of LA at 333 nm completely disappeared for cRGD-rPTM (Figure S1), signifying efficient ring-opening of dithiolane and crosslinking of micelles. Recent studies disclosed that nanomedicines with 20 mol % cRGD on

Table 1. Synthesis of PEG-*b*-PTyr-LA

		LA/PEG-PTyr (mol/mol)		M_n (kg/mol)		
entry	polymer	feed ratio	^{1}H NMR[a]	^{1}H NMR[a]	GPC[b]	$Đ$[b]
1	PEG-*b*-PTyr-LA$_4$	6.0	4.3	7.9	11.9	1.06
2	PEG-*b*-PTyr-LA$_8$	12.0	8.2	8.7	12.1	1.17

[a]Calculated from ^{1}H NMR. [b]Determined by GPC.

DOI: 10.1021/acs.biomac.8b00835
Biomacromolecules 2018, 19, 3586−3593

Table 2. Characterization of Dox-Loaded rPTM and cRGD-rPTM

		DLC (wt %)					
entry	NPs	theo.	determ.[a]	DLE[a] (%)	size[b] (nm)	PDI[b]	ξ[c] (mV)
1	cRGD-rPTM	10.0	9.1	89.6	44	0.15	−3.6
2	cRGD-rPTM	15.0	14.0	92.2	46	0.17	−3.8
3	cRGD-rPTM	20.0	18.5	90.7	45	0.04	−3.9
4	rPTM	20.0	18.8	92.5	42	0.06	−3.3

[a]Determined by fluorescence measurement. [b]Determined by DLS (1 mg/mL, 25 °C). [c]Determined by electrophoresis in HEPES (1 mg/mL, 25 °C).

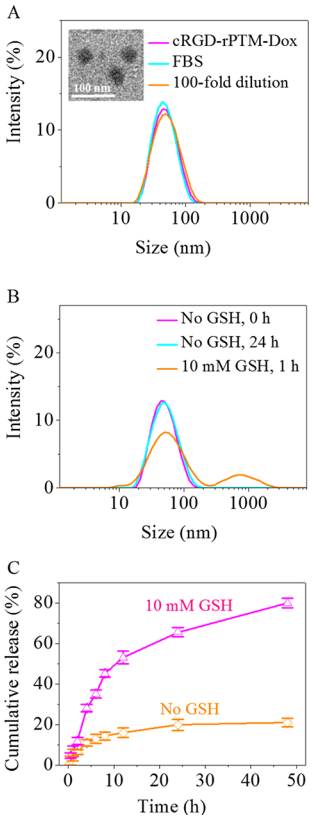

Figure 2. Characterization of cRGD-rPTM-Dox. (A) Size changes of cRGD-rPTM-Dox (1 mg/mL) against 100-dilution and 10% FBS at 25 °C determined by DLS. Inset was TEM image of cRGD-rPTM-Dox stained by phosphotungstic acid. (B) Size changes of cRGD-rPTM-Dox in HEPES buffer with 10 mM GSH. (C) In vitro drug release from cRGD-rPTM-Dox.

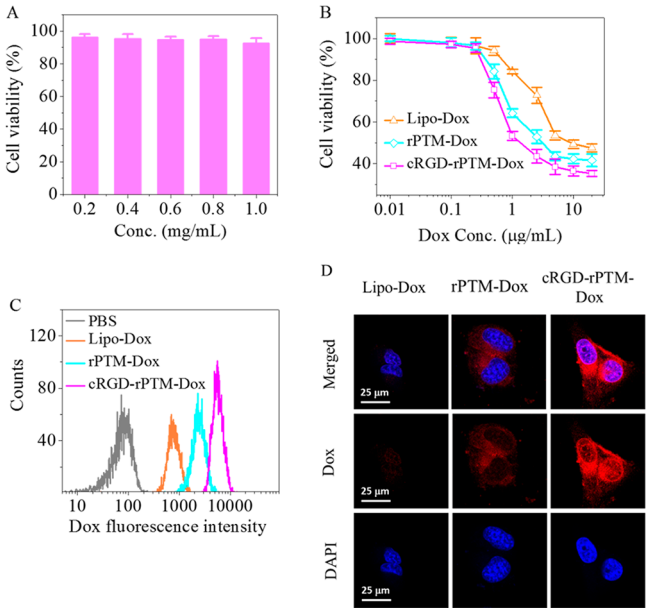

Figure 3. In vitro antitumor effect and cellular uptake in MDA-MB-231 breast cancer cells. (A) Cytotoxicity of blank cRGD-rPTM following 48 h treatment with cells. (B) In vitro antitumor efficacy of cRGD-rPTM-Dox, rPTM-Dox and Lipo-Dox. Cells were treated with different formulations for 0.5 h and further cultured in fresh media for another 71.5 h. (C) Flow cytometry assay. (D) CLSM images. Cells in both (C) and (D) were treated with cRGD-rPTM-Dox, rPTM-Dox, or Lipo-Dox (Dox dosage: 20.0 μg/mL) for 0.5 h.

the surface exhibited an optimal tumor targetability to $\alpha_v\beta_3$ positive tumor cells like U87MG glioma cells, A549 lung cancer cells, and B16F10 melanoma cells.[35,40,42,43] cRGD-rPTM displayed a small size of 40 nm with a low polydispersity index (PDI = 0.10; Figure S2) and a β-sheet structure (Figure S3). Of note, cRGD-rPTM exhibited a decent Dox loading efficiency of over 90% at theoretical DLC of 15 and 20 wt % (Table 2), likely owing to the intense $\pi-\pi$ interactions of Dox with tyrosine moieties in micellar cores, as previously reported for phenyl and naphthyl-functionaized micelles.[44−46] cRGD-rPTM-Dox even at 18.5 wt % Dox loading maintained a small hydrodynamic size of 45 nm (Figure 2A). Its small size was further confirmed by TEM. The size of nanomedicines plays a pivotal role in their tumor accumulation and penetration, as well as cellular uptake. Nanomedicines with particle sizes close to 50 nm have been reported to induce superior cancer treatment effect owing to efficient cellular uptake, deep tumor tissue penetration, and high tumor tissue retention.[47−51] The nontargeting rPTM-Dox control exhibited similar size and drug loading levels (Table 2). Both cRGD-rPTM-Dox and rPTM-Dox revealed a near neutral surface charge (−3.3 to −3.9 mV; Table 2), indicating that cRGD functionalization has little influence on its surface properties. cRGD-rPTM-Dox displayed little size change against 100-fold dilution, 10% FBS, and long-term storage (Figures 2A and S4), signifying its high stability. In contrast, noncrosslinked micelles, cRGD-PTM-Dox, displayed obviously enlarged sizes following 100-fold dilution (Figure S5), corroborating that crosslinking is critical in stabilizing micelles. Under reductive conditions (10 mM GSH), cRGD-rPTM-Dox swelled or aggregated in 1 h (Figure 2B). In comparison, in the presence of proteinase K (6 U mL^{-1}), cRGD-rPTM-Dox formed large particles in 12 h (Figure S6).

Figure 2C shows that around 20 and 80% of Dox was released from cRGD-rPTM-Dox in 48 h under physiological conditions in the absence and presence of GSH, respectively, supporting that a cytoplasmic reductive environment is an efficient trigger for drug release from cRGD-rPTM-Dox. The drug release could also be triggered by proteinase K (Figure

DOI: 10.1021/acs.biomac.8b00835
Biomacromolecules 2018, 19, 3586−3593

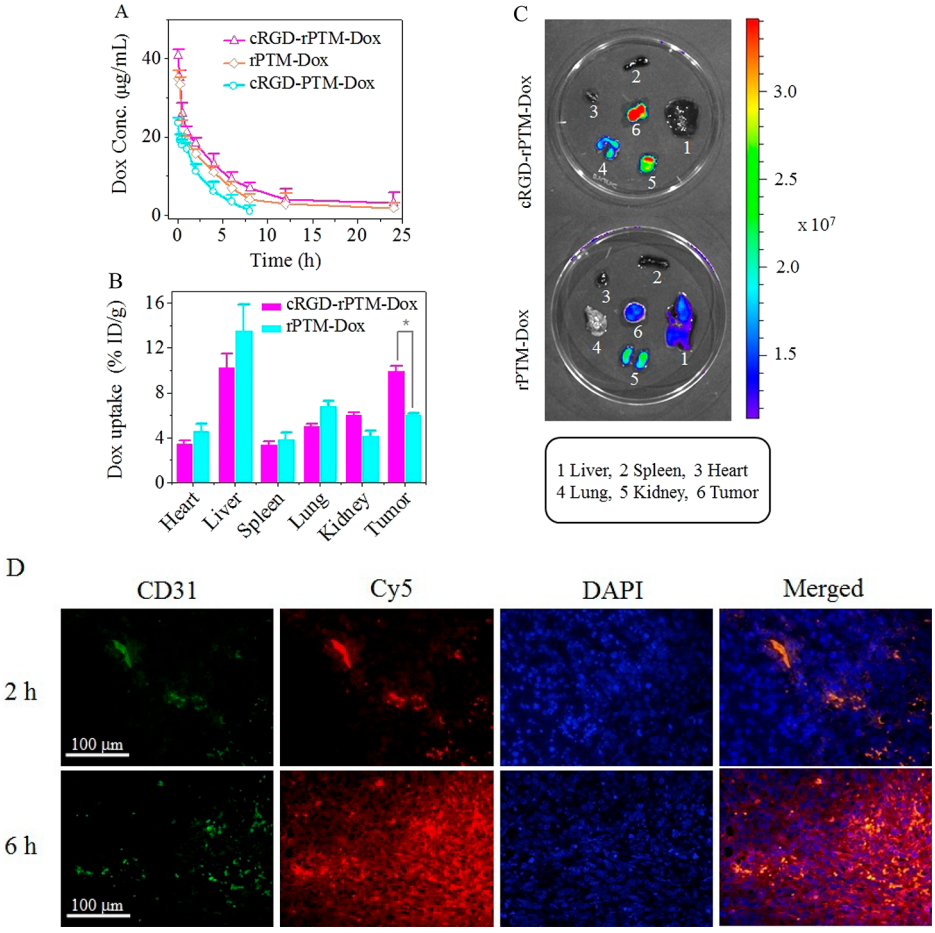

Figure 4. (A) In vivo pharmacokinetics in Balb/c mice. (B) In vivo biodistribution of Dox following 6 h postinjection in MDA-MB-231 tumor bearing nude mice (n = 3, *p < 0.05). (C) Dox fluorescence images of tumors and major organs harvested from MDA-MB-231 tumor xenografts following 6 h postinjection of different formulations. (D) Tumor penetration of Cy5 labeled cRGD-rPTM in tumor tissue at 2 and 6 h postinjection. The nuclei and blood vessels were stained with DAPI (blue) and CD31 (green), respectively.

S7). Interestingly, around 45 and 93% Dox was release in 48 h from cRGD-rPTM-Dox in proteinase K and proteinase K plus DTT, respectively.

In Vitro Antitumor Activity, Cellular Uptake, and Intracellular Trafficking. The cytotoxicity of blank and Dox-loaded cRGD-rPTM was evaluated in $\alpha_v\beta_3$ overexpressing MDA-MB-231 breast cancer cells. Cells treated with blank cRGD-rPTM at varying concentrations of 0.2−1.0 mg/mL displayed over 90% cell viability (Figure 3A), supporting that polypeptide micelles have little cytotoxicity. In comparison, both rPTM-Dox and cRGD-rPTM-Dox demonstrated a high anticancer activity with a half-maximal inhibitory concentration (IC_{50}) of 3.1 ± 0.4 and 1.5 ± 0.4 μg Dox equiv/mL, respectively (Figure 3B). Of note, cRGD-rPTM-Dox was significantly more potent than clinically used Lipo-Dox (IC_{50} = 10.1 ± 1.2 μg Dox equiv/mL), likely as a result of fast internalization and intracellular drug release. Flow cytometry revealed that MDA-MB-231 cells treated with cRGD-rPTM-Dox had 2.3-fold higher Dox fluorescence intensity than those with nontargeting rPTM-Dox (Figure 3C), confirming that cRGD-rPTM-Dox predominantly internalizes into cells via $\alpha_v\beta_3$ integrin-mediated mechanism.[35−38] Interestingly, confocal microscopy showed that strong Dox fluorescence was distributed throughout MDA-MB-231 cells including cell nuclei following just 0.5 h treatment with cRGD-rPTM-Dox (Figure 3D). In contrast, faint and little Dox fluorescence was detected in cells treated with rPTM-Dox and Lipo-Dox, respectively. These results further corroborate that cRGD-rPTM-Dox can actively target to $\alpha_v\beta_3$-integrin positive MDA-MB-231 cells and achieve quick drug release in the cytosol and cell nuclei, giving potent antitumor effect.

In Vivo Pharmacokinetics, Biodistribution, and Tumor Penetration. Encouraged by their high stability, cellular uptake, and cytotoxicity, we further evaluate the in vivo pharmacokinetics, biodistribution, and tumor penetration of cRGD-rPTM-Dox. The results showed that disulfide cross-linked micelles (rPTM-Dox and cRGD-rPTM-Dox) had prolonged circulation time with an elimination phase half-life of around 3.6 h, which was much longer than that of noncrosslinked cRGD-PTM-Dox (2.2 h; Figure 4A), signifying that disulfide-crosslinking plays a critical role in stabilizing the micelles and achieving long circulation. Figure 4B revealed that cRGD-rPTM-Dox had a pronounced Dox accumulation (9.96% ID/g) in MDA-MB-231 tumor xenografts following 6 h injection, which was remarkably higher than rPTM-Dox. Meanwhile, cRGD-rPTM-Dox displayed lower Dox accumulation in major organs (heart, liver, spleen, lung, etc.), signifying that cRGD-rPTM-Dox could possibly alleviate cardiotoxicity, which was reported to be the major side effect of free Dox.[52,53] Notably, kidney showed somewhat higher uptake of cRGD-rPTM-Dox than spleen, probably owing to binding of cRGD-rPTM-Dox to podocytes that are found to

DOI: 10.1021/acs.biomac.8b00835
Biomacromolecules 2018, 19, 3586−3593

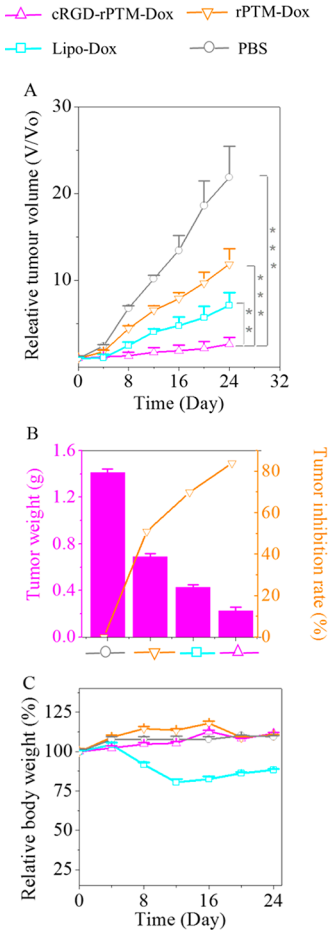

Figure 5. In vivo antitumor efficacy of cRGD-rPTM-Dox. (A) Tumor volume changes. cRGD-rPTM-Dox and rPTM-Dox were administered at a dosage of 6 mg Dox equiv/kg, while Lipo-Dox at a dosage of 4 mg Dox equiv/kg (n = 5, *p < 0.001). (B) Tumor weight and tumor inhibition rate of mice treated with different formulations on day 24. (C) Relative body weight changes of mice within 24 d (n = 6).

overexpress $\alpha_v\beta_3$ integrin.[54,55] The ex vivo fluorescence imaging demonstrated that, in comparison with rPTM-Dox, cRGD-rPTM-Dox presented remarkably stronger Dox fluorescence in tumor blocks, while much less Dox accumulation in healthy organs (Figure 4C). This coincides with previous studies of nanomedicines with small sizes of around 50 nm, which often display superior tumor accumulation as a result from deep tumor penetration and efficient internalization in cancer cells.[49−51] Notably, drug distribution in different organs is not totally consistent with the fluorescence intensity of Dox observed by ex vivo imaging, due to the fact that the fluorescence mainly derives from released Dox, while drug accumulation in different organs encompasses both released and unreleased Dox in micelles. Immunofluorescent analysis was employed to assess the tumor penetration of Cy5-cRGD-rPTM in MDA-MB-231 tumor-bearing nude mice according to previous reports.[56,57] As shown in Figure 4D, the smart polytyrosine micelles mainly colocalized with blood vessels following 2 h postadministration and could extravasate from tumor vasculature into the tumor tissue within 6 h. The remarkable tumor penetration of cRGD-rPTM could be attributed to their small sizes (~45 nm) and active tumor targetability.

In Vivo Therapeutic Efficacy. The in vivo therapeutic efficacy of cRGD-rPTM-Dox was explored in MDA-MB-231 tumor-bearing nude mice. The results demonstrated that cRGD-rPTM-Dox could almost completely suppress tumor growth at a dosage of 6 mg Dox equiv/kg, significantly outperforming both nontargeted counterpart (rPTM-Dox) and Lipo-Dox (Figure 5A). Figure 5B shows that cRGD-rPTM-Dox group had the smallest tumors among all the groups, in which a high tumor inhibition rate (TIR) of 84.2% was observed for cRGD-rPTM-Dox. In comparison, Lipo-Dox and rPTM-Dox groups had a TIR of 69.8% and 51.0%, respectively. Importantly, cRGD-rPTM-Dox group exhibited no body weight loss (Figure 5C), signifying that no obvious systemic toxicity was induced by cRGD-rPTM-Dox. In contrast, Lipo-Dox at a low dose of 4 mg Dox equiv/kg caused over 20% body weight loss and serious hand-food syndrome as from day 12. H&E staining clearly exhibited that cRGD-rPTM-Dox generated significantly more widespread tumor cell necrosis than Lipo-Dox (Figure S8). Meanwhile, unlike Lipo-Dox that induced significant damage to liver and heart, cRGD-rPTM-Dox group exhibited little injury to healthy organs. It is evident that cRGD-rPTM-Dox affords not only better therapeutic efficacy toward human breast tumor but also markedly reduced systemic toxicity compared with Lipo-Dox.

CONCLUSION

We have demonstrated that poly(ethylene glycol)-*b*-poly(L-tyrosine)-lipoic acid conjugates formed small-sized, robust and reduction-responsive micelles (rPTM) that achieve high and stable loading of lipophilic doxorubicin (Dox). The present study, using cRGD as a model targeting ligand and $\alpha_v\beta_3$ integrin positive MDA-MB-231 breast tumor model, shows that Dox-loaded cRGD-rPTM boosts a prolonged circulation time, selective and enhanced tumor retention, and remarkable tumor penetration. Notably, Dox-loaded cRGD-rPTM could effectively suppress growth of MDA-MB-231 human breast tumor at 6 mg Dox equiv/kg without inducing obvious side effects, significantly outperforming both nontargeted rPTM-Dox and clinically used LP-Dox controls. These multifunctional polytyrosine micelles are simple and easy to fabricate and could be decorated with different ligands, which renders them an interesting nanoplatform for targeted chemotherapy.

ASSOCIATED CONTENT

Supporting Information

The Supporting Information is available free of charge on the ACS Publications website at DOI: 10.1021/acs.biomac.8b00835.

Experimental on materials, characterization, in vitro release, MTT assay, cellular uptake, pharmacokinetics, biodistribution, and tumor penetration; size distribution and circular dichroism spectra of micelles; H&E staining (PDF).

AUTHOR INFORMATION

Corresponding Authors

*Tel.: +86-512-65884933. E-mail: cdeng@suda.edu.cn.
*Tel.: +86-512-65880098. E-mail: zyzhong@suda.edu.cn.

ORCID

Chao Deng: 0000-0001-7697-9874
Zhiyuan Zhong: 0000-0003-4175-4741

DOI: 10.1021/acs.biomac.8b00835
Biomacromolecules 2018, 19, 3586−3593

Author Contributions

The manuscript was written through contributions of all authors. All authors have given approval to the final version of the manuscript.

Notes

The authors declare no competing financial interest.

■ ACKNOWLEDGMENTS

This work was supported by the National Natural Science Foundation of China (NSFC 51773145, 51473110, 51633005, and 51761135117).

■ REFERENCES

(1) Chen, H.; Zhang, W.; Zhu, G.; Xie, J.; Chen, X. Rethinking Cancer Nanotheranostics. *Nat. Rev. Mater.* **2017**, *2*, 17024.
(2) Kamaly, N.; Yameen, B.; Wu, J.; Farokhzad, O. C. Degradable Controlled-Release Polymers and Polymeric Nanoparticles: Mechanisms of Controlling Drug Release. *Chem. Rev.* **2016**, *116*, 2602−2663.
(3) Tang, Z.; He, C.; Tian, H.; Ding, J.; Hsiao, B. S.; Chu, B.; Chen, X. Polymeric Nanostructured Materials for Biomedical Applications. *Prog. Polym. Sci.* **2016**, *60*, 86−128.
(4) Song, Z.; Han, Z.; Lv, S.; Chen, C.; Chen, L.; Yin, L.; Cheng, J. Synthetic Polypeptides: From Polymer Design to Supramolecular Assembly and Biomedical Application. *Chem. Soc. Rev.* **2017**, *46*, 6570−6599.
(5) Mochida, Y.; Cabral, H.; Kataoka, K. Polymeric Micelles for Targeted Tumor Therapy of Platinum Anticancer Drugs. *Expert Opin. Drug Delivery* **2017**, *14*, 1423−1438.
(6) Deming, T. J. Synthesis of Side-Chain Modified Polypeptides. *Chem. Rev.* **2016**, *116*, 786−808.
(7) He, C.; Zhuang, X.; Tang, Z.; Tian, H.; Chen, X. Stimuli-Sensitive Synthetic Polypeptide-Based Materials for Drug and Gene Delivery. *Adv. Healthcare Mater.* **2012**, *1*, 48−78.
(8) Deng, C.; Wu, J.; Cheng, R.; Meng, F.; Klok, H.-A.; Zhong, Z. Functional Polypeptide and Hybrid Materials: Precision Synthesis Via Alpha-Amino Acid N-Carboxyanhydride Polymerization and Emerging Biomedical Applications. *Prog. Polym. Sci.* **2014**, *39*, 330−364.
(9) Bonduelle, C.; Oliveira, H.; Gauche, C.; Huang, J.; Heise, A.; Lecommandoux, S. Multivalent Effect of Glycopolypeptide Based Nanoparticles for Galectin Binding. *Chem. Commun.* **2016**, *52*, 11251−11254.
(10) Cabral, H.; Kataoka, K. Progress of Drug-Loaded Polymeric Micelles into Clinical Studies. *J. Controlled Release* **2014**, *190*, 465−476.
(11) Wicki, A.; Witzigmann, D.; Balasubramanian, V.; Huwyler, J. Nanomedicine in Cancer Therapy: Challenges, Opportunities, and Clinical Applications. *J. Controlled Release* **2015**, *200*, 138−157.
(12) Deng, C.; Jiang, Y.; Cheng, R.; Meng, F.; Zhong, Z. Biodegradable Polymeric Micelles for Targeted and Controlled Anticancer Drug Delivery: Promises, Progress and Prospects. *Nano Today* **2012**, *7*, 467−480.
(13) Shi, J.; Kantoff, P. W.; Wooster, R.; Farokhzad, O. C. Cancer Nanomedicine: Progress, Challenges and Opportunities. *Nat. Rev. Cancer* **2017**, *17*, 20−37.
(14) Talelli, M.; Barz, M.; Rijcken, C. J. F.; Kiessling, F.; Hennink, W. E.; Lammers, T. Core-Crosslinked Polymeric Micelles: Principles, Preparation, Biomedical Applications and Clinical Translation. *Nano Today* **2015**, *10*, 93−117.
(15) Hare, J. I.; Lammers, T.; Ashford, M. B.; Puri, S.; Storm, G.; Barry, S. T. Challenges and Strategies in Anti-Cancer Nanomedicine Development: An Industry Perspective. *Adv. Drug Delivery Rev.* **2017**, *108*, 25−38.
(16) Li, Y.; Xiao, K.; Zhu, W.; Deng, W.; Lam, K. S. Stimuli-Responsive Cross-Linked Micelles for on-Demand Drug Delivery against Cancers. *Adv. Drug Delivery Rev.* **2014**, *66*, 58−73.
(17) Elsabahy, M.; Heo, G. S.; Lim, S.-M.; Sun, G.; Wooley, K. L. Polymeric Nanostructures for Imaging and Therapy. *Chem. Rev.* **2015**, *115*, 10967−11011.
(18) Sun, H.; Meng, F.; Cheng, R.; Deng, C.; Zhong, Z. Reduction-Sensitive Degradable Micellar Nanoparticles as Smart and Intuitive Delivery Systems for Cancer Chemotherapy. *Expert Opin. Drug Delivery* **2013**, *10*, 1109−1122.
(19) Xiao, K.; Liu, Q.; Al Awwad, N.; Zhang, H.; Lai, L.; Luo, Y.; Lee, J. S.; Li, Y.; Lam, K. S. Reversibly Disulfide Cross-Linked Micelles Improve the Pharmacokinetics and Facilitate the Targeted, on-Demand Delivery of Doxorubicin in the Treatment of B-Cell Lymphoma. *Nanoscale* **2018**, *10*, 8207−8216.
(20) Yu, S.; Ding, J.; He, C.; Cao, Y.; Xu, W.; Chen, X. Disulfide Cross-Linked Polyurethane Micelles as a Reduction-Triggered Drug Delivery System for Cancer Therapy. *Adv. Healthcare Mater.* **2014**, *3*, 752−760.
(21) Deng, Z.; Yuan, S.; Xu, R. X.; Liang, H.; Liu, S. Reduction-Triggered Transformation of Crosslinking Modules of Disulfide-Containing Micelles with Chemically Tunable Rates. *Angew. Chem., Int. Ed.* **2018**, *57*, 8896−8900.
(22) Ruttala, H. B.; Chitrapriya, N.; Kaliraj, K.; Ramasamy, T.; Shin, W. H.; Jeong, J.-H.; Kim, J. R.; Ku, S. K.; Choi, H.-G.; Yong, C. S.; Kim, J. O. Facile Construction of Bioreducible Crosslinked Polypeptide Micelles for Enhanced Cancer Combination Therapy. *Acta Biomater.* **2017**, *63*, 135−149.
(23) Hsiao, L.-W.; Lai, Y.-D.; Lai, J.-T.; Hsu, C.-C.; Wang, N.-Y.; Steven, S. S. W.; Jan, J.-S. Cross-Linked Polypeptide-Based Gel Particles by Emulsion for Efficient Protein Encapsulation. *Polymer* **2017**, *115*, 261−272.
(24) Oe, Y.; Christie, R. J.; Naito, M.; Low, S. A.; Fukushima, S.; Toh, K.; Miura, Y.; Matsumoto, Y.; Nishiyama, N.; Miyata, K.; Kataoka, K. Actively-Targeted Polyion Complex Micelles Stabilized by Cholesterol and Disulfide Cross-Linking for Systemic Delivery of siRNA to Solid Tumors. *Biomaterials* **2014**, *35*, 7887−7895.
(25) Sun, J.; Chen, X.; Lu, T.; Liu, S.; Tian, H.; Guo, Z.; Jing, X. Formation of Reversible Shell Cross-Linked Micelles from the Biodegradable Amphiphilic Diblock Copolymer Poly(L-Cysteine)-Block-Poly(L-Lactide). *Langmuir* **2008**, *24*, 10099−10106.
(26) Zheng, N.; Song, Z.; Liu, Y.; Zhang, R.; Zhang, R.; Yao, C.; Uckun, F. M.; Yin, L.; Cheng, J. Redox-Responsive, Reversibly-Crosslinked Thiolated Cationic Helical Polypeptides for Efficient siRNA Encapsulation and Delivery. *J. Controlled Release* **2015**, *205*, 231−239.
(27) Li, J.; Yu, X.; Wang, Y.; Yuan, Y.; Xiao, H.; Cheng, D.; Shuai, X. A Reduction and pH Dual-Sensitive Polymeric Vector for Long-Circulating and Tumor-Targeted Sirna Delivery. *Adv. Mater.* **2014**, *26*, 8217−8224.
(28) Huang, K.; Shi, B.; Xu, W.; Ding, J.; Yang, Y.; Liu, H.; Zhuang, X.; Chen, X. Reduction-Responsive Polypeptide Nanogel Delivers Antitumor Drug for Improved Efficacy and Safety. *Acta Biomater.* **2015**, *27*, 179−193.
(29) Guo, H.; Xu, W.; Chen, J.; Yan, L.; Ding, J.; Hou, Y.; Chen, X. Positively Charged Polypeptide Nanogel Enhances Mucoadhesion and Penetrability of 10-Hydroxycamptothecin in Orthotopic Bladder Carcinoma. *J. Controlled Release* **2017**, *259*, 136−148.
(30) Jing, T.; Fu, L.; Liu, L.; Yan, L. A Reduction-Responsive Polypeptide Nanogel Encapsulating NIR Photosensitizer for Imaging Guided Photodynamic Therapy. *Polym. Chem.* **2016**, *7*, 951−957.
(31) Gu, X.; Qiu, M.; Sun, H.; Zhang, J.; Cheng, L.; Deng, C.; Zhong, Z. Polytyrosine Nanoparticles Enable Ultra-High Loading of Doxorubicin and Rapid Enzyme-Responsive Drug Release. *Biomater. Sci.* **2018**, *6*, 1526−1534.
(32) Yang, W.; Zou, Y.; Meng, F.; Zhang, J.; Cheng, R.; Deng, C.; Zhong, Z. Efficient and Targeted Suppression of Human Lung Tumor Xenografts in Mice with Methotrexate Sodium Encapsulated in All-Function-in-One Chimeric Polymersomes. *Adv. Mater.* **2016**, *28*, 8234−8239.
(33) Li, Y.-L.; Zhu, L.; Liu, Z.; Cheng, R.; Meng, F.; Cui, J.-H.; Ji, S.-J.; Zhong, Z. Reversibly Stabilized Multifunctional Dextran Nano-

DOI: 10.1021/acs.biomac.8b00835
Biomacromolecules 2018, 19, 3586−3593

particles Efficiently Deliver Doxorubicin into the Nuclei of Cancer Cells. *Angew. Chem., Int. Ed.* **2009**, *48*, 9914−9918.
(34) Sun, B.; Deng, C.; Meng, F.; Zhang, J.; Zhong, Z. Robust, Active Tumor-Targeting and Fast Bioresponsive Anticancer Nanotherapeutics Based on Natural Endogenous Materials. *Acta Biomater.* **2016**, *45*, 223−233.
(35) Quader, S.; Liu, X.; Chen, Y.; Mi, P.; Chida, T.; Ishii, T.; Miura, Y.; Nishiyama, N.; Cabral, H.; Kataoka, K. cRGD Peptide-Installed Epirubicin-Loaded Polymeric Micelles for Effective Targeted Therapy against Brain Tumors. *J. Controlled Release* **2017**, *258*, 56−66.
(36) Qiu, M.; Ouyang, J.; Sun, H.; Meng, F.; Cheng, R.; Zhang, J.; Cheng, L.; Lan, Q.; Deng, C.; Zhong, Z. Biodegradable Micelles Based on Poly(Ethylene Glycol)-b-Polylipopepide Copolymer: A Robust and Versatile Nanoplatform for Anticancer Drug Delivery. *ACS Appl. Mater. Interfaces* **2017**, *9*, 27587−27595.
(37) Miyano, K.; Cabral, H.; Miura, Y.; Matsumoto, Y.; Mochida, Y.; Kinoh, H.; Iwata, C.; Nagano, O.; Saya, H.; Nishiyama, N.; Kataoka, K.; Yamasoba, T. cRGD Peptide Installation on Cisplatin- Loaded Nanomedicines Enhances Efficacy against Locally Advanced Head and Neck Squamous Cell Carcinoma Bearing Cancer Stem-Like Cells. *J. Controlled Release* **2017**, *261*, 275−286.
(38) Song, W.; Tang, Z.; Zhang, D.; Zhang, Y.; Yu, H.; Li, M.; Lv, S.; Sun, H.; Deng, M.; Chen, X. Anti-Tumor Efficacy of c(RGDfK)-Decorated Polypeptide-Based Micelles Co-Loaded with Docetaxel and Cisplatin. *Biomaterials* **2014**, *35*, 3005−3014.
(39) Wu, J.; Zhang, J.; Deng, C.; Meng, F.; Zhong, Z. Vitamin E-Oligo(Methyl Diglycol L-Glutamate) as a Biocompatible and Functional Surfactant for Facile Preparation of Active Tumor-Targeting PLGA Nanoparticles. *Biomacromolecules* **2016**, *17*, 2367−2374.
(40) Qiu, M.; Sun, H.; Meng, F.; Cheng, R.; Zhang, J.; Deng, C.; Zhong, Z. Lipopepsomes: A Novel and Robust Family of Nano-Vesicles Capable of Highly Efficient Encapsulation and Tumor-Targeted Delivery of Doxorubicin Hydrochloride in Vivo. *J. Controlled Release* **2018**, *272*, 107−113.
(41) Fang, Y.; Jiang, Y.; Zou, Y.; Meng, F.; Zhang, J.; Deng, C.; Sun, H.; Zhong, Z. Targeted Glioma Chemotherapy by Cyclic RGD Peptide-Functionalized Reversibly Core-Crosslinked Multifunctional Poly(Ethylene Glycol)-b-Poly (Epsilon-Caprolactone) Micelles. *Acta Biomater.* **2017**, *50*, 396−406.
(42) Guo, Y.; Niu, B.; Song, Q.; Zhao, Y.; Bao, Y.; Tan, S.; Si, L.; Zhang, Z. RGD-Decorated Redox-Responsive D-Alpha-Tocopherol Polyethylene Glycol Succinate-Poly(Lactide) Nanoparticles for Targeted Drug Delivery. *J. Mater. Chem. B* **2016**, *4*, 2338−2350.
(43) Zhu, Y.; Jian, Z.; Meng, F.; Chao, D.; Ru, C.; Jan, F.; Zhong, Z. cRGD/TAT Dual-Ligand Reversibly Cross-Linked Micelles Loaded with Docetaxel Penetrate Deeply into Tumor Tissue and Show High Antitumor Efficacy in Vivo. *ACS Appl. Mater. Interfaces* **2017**, *9*, 35651−35663.
(44) Shi, Y.; van Steenbergen, M. J.; Teunissen, E. A.; Novo, L.; Gradmann, S.; Baldus, M.; van Nostrum, C. F.; Hennink, W. E. Pi-Pi Stacking Increases the Stability and Loading Capacity of Thermosensitive Polymeric Micelles for Chemotherapeutic Drugs. *Biomacromolecules* **2013**, *14*, 1826−1837.
(45) Liang, Y.; Deng, X.; Zhang, L.; Peng, X.; Gao, W.; Cao, J.; Gu, Z.; He, B. Terminal Modification of Polymeric Micelles with Pi-Conjugated Moieties for Efficient Anticancer Drug Delivery. *Biomaterials* **2015**, *71*, 1−10.
(46) Varghese, O. P.; Liu, J.; Sundaram, K.; Hilborn, J.; Oommen, O. P. Chondroitin Sulfate Derived Theranostic Nanoparticles for Targeted Drug Delivery. *Biomater. Sci.* **2016**, *4*, 1310−1313.
(47) Cabral, H.; Matsumoto, Y.; Mizuno, K.; Chen, Q.; Murakami, M.; Kimura, M.; Terada, Y.; Kano, M. R.; Miyazono, K.; Uesaka, M.; Nishiyama, N.; Kataoka, K. Accumulation of Sub-100 nm Polymeric Micelles in Poorly Permeable Tumours Depends on Size. *Nat. Nanotechnol.* **2011**, *6*, 815−823.
(48) Wang, J.; Mao, W.; Lock, L. L.; Tang, J.; Sui, M.; Sun, W.; Cui, H.; Xu, D.; Shen, Y. The Role of Micelle Size in Tumor Accumulation, Penetration, and Treatment. *ACS Nano* **2015**, *9*, 7195−7206.
(49) Tang, L.; Yang, X.; Yin, Q.; Cai, K.; Wang, H.; Chaudhury, I.; Yao, C.; Zhou, Q.; Kwon, M.; Hartman, J. A.; Dobrucki, I. T.; Dobrucki, L. W.; Borst, L. B.; Lezmig, S.; Helferich, W. G.; Ferguson, A. L.; Fan, T. M.; Cheng, J. Investigating the Optimal Size of Anticancer Nanomedicine. *Proc. Natl. Acad. Sci. U. S. A.* **2014**, *111*, 15344−15349.
(50) Huo, S.; Ma, H.; Huang, K.; Liu, J.; Wei, T.; Jin, S.; Zhang, J.; He, S.; Liang, X.-J. Superior Penetration and Retention Behavior of 50 nm Gold Nanoparticles in Tumors. *Cancer Res.* **2013**, *73*, 319−330.
(51) Perry, J. L.; Reuter, K. G.; Luft, J. C.; Pecot, C. V.; Zamboni, W.; DeSimone, J. M. Mediating Passive Tumor Accumulation through Particle Size, Tumor Type, and Location. *Nano Lett.* **2017**, *17*, 2879−2886.
(52) Tahover, E.; Patil, Y. P.; Gabizon, A. A. Emerging Delivery Systems to Reduce Doxorubicin Cardiotoxicity and Improve Therapeutic Index: Focus on Liposomes. *Anti-Cancer Drugs* **2015**, *26*, 241−258.
(53) Lien, C.-Y.; Jensen, B. T.; Chen, M.-L.; Wu, C.-H.; Lin, C.-L.; Chuang, T.-Y. The Effect of Endurance Exercise on Doxorubicin Cardiotoxicity and Antitumor Efficacy in Tumor-Bearing Mice. *FASEB J.* **2016**, *30*, 1288.
(54) Wang, J.; Masehi-Lano, J. J.; Chung, E. J. Peptide and Antibody Ligands for Renal Targeting: Nanomedicine Strategies for Kidney Disease. *Biomater. Sci.* **2017**, *5*, 1450−1459.
(55) Pollinger, K.; Hennig, R.; Breunig, M.; Tessmar, J.; Ohlmann, A.; Tamm, E. R.; Witzgall, R.; Goepferich, A. Kidney Podocytes as Specific Targets for Cyclo(RGDfC)-Modified Nanoparticles. *Small* **2012**, *8*, 3368−3375.
(56) Chen, J.; Zou, Y.; Deng, C.; Meng, F.; Zhang, J.; Zhong, Z. Multifunctional Click Hyaluronic Acid Nanogels for Targeted Protein Delivery and Effective Cancer Treatment in Vivo. *Chem. Mater.* **2016**, *28*, 8792−8799.
(57) Zhu, Y.; Jiang, Y.; Meng, F.; Deng, C.; Cheng, R.; Zhang, J.; Feijen, J.; Zhong, Z. Highly Efficacious and Specific Anti-Glioma Chemotherapy by Tandem Nanomicelles Co-Functionalized with Brain Tumor-Targeting and Cell-Penetrating Peptides. *J. Controlled Release* **2018**, *278*, 1−8.

DOI: 10.1021/acs.biomac.8b00835
Biomacromolecules 2018, 19, 3586−3593